Shear-layer acoustic radiation in an excited subsonic jet: models for vortex pairing and superdirective noise

Vincent Fleury, Christophe Bailly *, Daniel Juvé

*Laboratoire de mécanique des fluides et d'acoustique, UMR CNRS 5509 & École centrale de Lyon,
36, avenue Guy de Collongue, 69134 Ecully cedex, France*

Presented by Geneviève Comte-Bellot

Abstract

The pressure field generated by a cylindrical boundary pressure wave with spatial modulation is calculated. This model is confronted to the experimental results in order to explain the two observed radiation patterns associated with subharmonic fluctuations in an excited jet shear-layer, namely either a superdirective emission, or a vortex pairing type of radiation with extinction angle. Regarding the far field, the superdirective pattern is recovered by using a generalized Gaussian as a modulation function and the vortex pairing features by a two lobe sinusoidal modulation, in agreement with the experimental description of the near pressure field. Regarding the near field, its exponential decay is also recovered in both cases. *To cite this article: V. Fleury et al., C. R. Mecanique 333 (2005).*
© 2005 Académie des sciences. Published by Elsevier SAS. All rights reserved.

Résumé

Rayonnement acoustique de la couche de cisaillement d'un jet excité subsonique : modèles pour le bruit d'appariement tourbillonaire et superdirectif. Le champ de pression produit par une condition aux limites de forme cylindrique constituée d'une onde de pression modulée spatialement est calculé. Ce modèle est confronté aux résultats expérimentaux relatés afin d'expliquer les deux types de rayonnement observés des fluctuations sous-harmoniques d'une couche de cisaillement d'un jet excité, à savoir soit une émission superdirective, soit un rayonnement d'appariement tourbillonnaire avec angle d'extinction. Concernant le champ lointain, le diagramme acoustique superdirectif est retrouvé en utilisant une gaussienne généralisée comme fonction de modulation et les caractéristiques du rayonnement d'appariement tourbillonnaire à l'aide d'une modulation formée de deux arches sinusoïdales, en accord avec la description expérimentale du champ proche. Concernant le champ proche, sa décroissance exponentielle est aussi retrouvée dans les deux cas. *Pour citer cet article : V. Fleury et al., C. R. Mecanique 333 (2005).*
© 2005 Académie des sciences. Published by Elsevier SAS. All rights reserved.

---

* Corresponding author.
   E-mail addresses: vincent.fleury@ec-lyon.fr (V. Fleury), christophe.bailly@ec-lyon.fr (C. Bailly).
   URL: http://acoustique.ec-lyon.fr (V. Fleury).

Version française abrégée

Le bruit émis par les fluctuations de la couche de cisaillement d'un jet excité a été étudié expérimentalement dans [1]. Deux types de rayonnement concernant le premier sous-harmonique ont été observés. Pour une vitesse $U_j = 20$ m·s^{-1}, le diagramme de directivité présente un angle d'extinction $\theta^\star$ à 85° de l'axe aval du jet, en accord avec les mesures de Bridges [2]. Pour $U_j = 40$ m·s^{-1}, le rayonnement est fortement orienté vers l'aval et correspond à une émission superdirective, comme observé par Laufer et Yen [3].

Cette étude vise à retrouver ces deux formes d'émission acoustique en calculant le rayonnement du champ de pression proche, à proximité du jet. Cette démarche suit l'approche de Crighton et Huerre [4]. Le champ de pression proche est défini sur une surface cylindrique en périphérie de jet par une onde modulée spatialement, de forme sinusoïdale ou gaussienne. Le champ acoustique lointain est obtenu en résolvant l'équation de propagation acoustique (2). Le résultat est donné par l'expression (6). En utilisant l'hypothèse de compacité radiale $k_{ac}r_j \ll 1$, l'expression simplifiée (7) est établie, où k_{ac} et r_j sont le nombre d'onde acoustique et le rayon du jet respectivement. Le champ proche incompressible est calculé en prenant $k_{ac} = 0$. Le résultat est donné par l'expression (8) et, pour une modulation spatiale lente, la forme asymptotique (9) est obtenue.

Ces résultats sont comparés aux données expérimentales rapportées dans [1]. Les paramètres impliqués dans ce modèle sont déterminés à l'aide des caractéristiques du champ proche données dans le tableau 3 de [1]. La directivité de type bruit d'appariement tourbillonnaire est alors retrouvée en considérant une fonction de modulation constituée deux arches de sinusoïde (15), comme indiqué dans [1]. En particulier, un angle d'extinction est trouvé pour $\theta^\star \approx 90°$, voir Fig. 1(c) and (d). L'émission superdirective est obtenue en utilisant la gaussienne généralisée $E_3(x)$ comme fonction d'enveloppe, donnée par l'expression (13) et Fig. 1(a) et (b).

Par ailleurs, la décroissance du champ de pression à proximité du jet est dans l'ensemble en bon accord avec l'atténuation exponentielle observée expérimentalement dans ces deux cas, voir Fig. 2.

1. Introduction

The subharmonic noise generated by an excited jet shear-layer has been investigated experimentally in a previous paper [1]. Two distinct acoustic radiation patterns of the first subharmonic pressure have been observed. For a velocity of $U_j = 20$ m·s^{-1}, a directivity pattern displaying an extinction angle $\theta^\star$ at 85° from the jet axis has been found, while for a velocity of $U_j = 40$ m·s^{-1}, a superdirective radiation strongly oriented downstream has been measured. The turbulent state of the initial shear-layer has been found discriminant. These two kinds of subharmonic radiation have already been reported in the literature by Bridges and Hussain [5] and Laufer and Yen [3], respectively. However, no unique view on the involved noise mechanism has been offered.

To explain the presence of an extinction angle $\theta^\star$, Bridges and Hussain [5] used an acoustic analogy theory and modeled the vortical source term as a compact quadrupolar acoustic emitter distributed axisymmetrically around the jet. Indeed, a similar extinction angle is then predicted, given by $3\cos^2\theta^\star - 1 = 0$ or $\theta^\star \simeq 55°$. Several arguments have been put forward by Bridges [2] and Bridges and Hussain [5] to explain the discrepancy about the location of $\theta^\star$: the effect of the initial conditions of the shear-layer on the evolution of the vortices and then on their acoustic radiation or a non perfectly compact source and thus an inappropriate decomposition of the acoustic source according to multipoles.

Laufer and Yen [3], on the other hand, proposed a wave-like description of subharmonic convective fluctuations in the shear-layer. This idea was then developed by Crighton and Huerre [4] in the framework of a wavy-wall radiation problem. Shear-layer pressure fluctuations are modelled by a wave, which is modulated by an envelope of large extent and of Gaussian form in following the observations of Laufer and Yen [3]. The superdirective emission pattern was thus recovered.

In the present study, this wavy-wall approach is followed and the occurrence of an extinction angle $\theta^\star$ in the far-field is studied through this theory. Furthermore, the analysis is made in axisymmetric geometry and the parameters involved in the description of the pressure wave in the shear-layer and its modulation are taken from the present experiments.

2. Analysis of the acoustic field generated by a cylindrical boundary pressure

The acoustic field radiated from a cylindrical boundary pressure into a quiescent medium is investigated. The boundary pressure is prescribed in $r = r_j = D/2$ as a traveling wave modulated by an envelope $E(x)$:

$$p'(x, r = r_j, t) = E(x) \exp\{i(k_x x - \omega t)\} \tag{1}$$

where ω and k_x are the pulsation and the axial wavenumber of the fluctuation, respectively. The pressure $p'(x, r, t)$ on the domain $r \geqslant r_j$ is thus sought as:

$$p'(x, r, t) = p(x, r) \exp(-i\omega t)$$

and the wave equation to solve can be written:

$$\left(\frac{\partial^2}{\partial x^2} + \frac{1}{r} \frac{\partial}{\partial r} + \frac{\partial^2}{\partial r^2} \right) p + k_{ac}^2 p = 0 \tag{2}$$

where $k_{ac} = \omega/c_\infty$ is the acoustic wavenumber and c_∞ the speed of sound. By taking the Fourier transform of $p(x, r)$ according to x:

$$\hat{p}(k, r) = \frac{1}{2\pi} \int\limits_{-\infty}^{+\infty} p(x, r) \exp(-ikx) \, dx$$

the solution of equation (2) is given by:

$$\hat{p}(k, r) = \begin{cases} C(k) H_0^1(ik_r r) & \text{if } |k| > k_{ac} \\ C(k) H_0^1(k_r r) & \text{otherwise} \end{cases} \tag{3}$$

where $k_r = \sqrt{|k_{ac}^2 - k^2|}$ is the transverse wavenumber and H_0^1 is the Hankel function of the first kind and zero order. The coefficient $C(k)$ is provided by the Fourier transform of the boundary condition (1):

$$C(k) = \begin{cases} \hat{E}(k - k_x)/H_0^1(ik_r r_j) & \text{if } |k| > k_{ac} \\ \hat{E}(k - k_x)/H_0^1(k_r r_j) & \text{otherwise} \end{cases} \tag{4}$$

The solution $p(x, r)$ to the problem (1) and (2) can then be obtained by taking the inverse Fourier transform of $\hat{p}(k, r)$. In the following, asymptotic expressions of the pressure $p(x, r)$ in the far and near fields are investigated.

Regarding the far field, i.e. $k_r r \gg 1$, $|\hat{p}(k, r)|$ decays as $1/\sqrt{r}$ for $|k| < k_{ac}$ and as $\exp(-k_r r)/\sqrt{r}$ for $|k| > k_{ac}$, see [6] for instance. Therefore, the contribution to the far acoustic field mainly results of components $|k| < k_{ac}$ and the pressure $p(x, r)$ reduces to:

$$p(x, r) \sim \int\limits_{-k_{ac}}^{+k_{ac}} \frac{\hat{E}(k - k_x)}{H_0^1(k_r r_j)} H_0^1(k_r r) \exp(ikx) \, dk \tag{5}$$

In order to estimate the directivity pattern, the spherical coordinates (R, θ) are introduced. The method of stationary phase then yields for $k_r R \sin\theta \gg 1$:

$$p(R, \theta) \sim \sqrt{2\pi} \frac{k_{ac} \hat{E}(k_{ac} \cos\theta - k_x)}{H_0^1(k_{ac} r_j \sin\theta)} \frac{\exp(ik_{ac} R + i\pi/4)}{k_{ac} R} \tag{6}$$

This expression can still be simplified by assuming a radial compactness condition $k_{ac} r_j \ll 1$. The term $H_0^1(k_{ac} r_j \sin\theta)$ is thus close to $2i \ln(k_{ac} r_j)/\pi$, and the expression (6) reads finally:

$$p(R, \theta) \sim \left(\frac{\pi}{2} \right)^{1/2} \frac{\pi}{\ln(k_{ac} r_j)} k_{ac} \hat{E}(k_{ac} \cos\theta - k_x) \frac{\exp(ik_{ac} R - i\pi/4)}{k_{ac} R} \tag{7}$$

Regarding the near pressure field, i.e. $k_{ac}|r - r_j| \ll 1$, compressibility effects are negligible and the problem governed by Eqs. (1) and (2) can be considered for $k_{ac} = 0$. The solution $\hat{p}(k, r)$ is then straightly deduced from expressions (3) and (4):

$$\hat{p}(k, r) = \frac{\hat{E}(k - k_x)}{H_0^1(\mathrm{i}|kr_j|)} H_0^1(\mathrm{i}|kr|)$$

and the near pressure field $p(x, r)$ reads:

$$p(x, r) = \int_{-\infty}^{+\infty} \frac{\hat{E}(k - k_x)}{H_0^1(\mathrm{i}|kr_j|)} H_0^1(\mathrm{i}|kr|) \exp(\mathrm{i}kx)\, \mathrm{d}k \tag{8}$$

It is interesting to evaluate this expression for a slowly spatially modulated boundary pressure (1), i.e. $\sigma_e/\lambda_x \gg 1$ or $\sigma_e k_x \gg 1$, with σ_e the typical length scale of $E(x)$ and $\lambda_x = 2\pi/k_x$ the wavelength of the pressure wave. By splitting the integral (8) according to positive and negative k wavenumbers and introducing the new variable $u = \sigma_e(k - k_x)$, the pressure $p(x, r)$ can be written:

$$p(x, r) = \exp(\mathrm{i}k_x x) \int_{-\sigma_e k_x}^{+\infty} \frac{\hat{E}(u/\sigma_e)}{H_0^1[\mathrm{i}(\sigma_e k_x + u)r_j/\sigma_e]} H_0^1\big[\mathrm{i}(\sigma_e k_x + u)r/\sigma_e\big] \exp\left(\mathrm{i}\frac{u}{\sigma_e}x\right) \frac{\mathrm{d}u}{\sigma_e}$$

$$+ \exp(\mathrm{i}k_x x) \int_{-\infty}^{-\sigma_e k_x} \frac{\hat{E}(u/\sigma_e)}{H_0^1[-\mathrm{i}(\sigma_e k_x + u)r_j/\sigma_e]} H_0^1\big[-\mathrm{i}(\sigma_e k_x + u)r/\sigma_e\big] \exp\left(\mathrm{i}\frac{u}{\sigma_e}x\right) \frac{\mathrm{d}u}{\sigma_e}$$

For $\sigma_e k_x \gg 1$, $p(x, r)$ is mainly given by the first integral, which can be evaluated by expanding the two Hankel functions H_0^1. Hence:

$$p(x, r) \sim \exp(\mathrm{i}k_x x) \int_{-\infty}^{+\infty} \hat{E}(u/\sigma_e) \frac{\exp(-(k_x + u/\sigma_e)r)/\sqrt{(k_x + u/\sigma_e)r}}{\exp(-(k_x + u/\sigma_e)r_j)/\sqrt{(k_x + u/\sigma_e)r_j}} \exp\left(\mathrm{i}\frac{u}{\sigma_e}x\right) \frac{\mathrm{d}u}{\sigma_e}$$

By introducing the variable $z = x + \mathrm{i}(r - r_j)$, the near pressure field reads finally:

$$p(x, r) \sim \sqrt{\frac{r_j}{r}} E(z) \exp(\mathrm{i}k_x z) \tag{9}$$

The boundary pressure in $r = r_j$ is thus analytically continued in the near-field $r \geqslant r_j$, with a $1/\sqrt{r}$ decay.

Expression (7) provides the acoustic far field and expressions (8) and (9) the near pressure field for a given boundary pressure condition (1). Expression (7) is valid for any boundary pressure (1) and especially, regardless of its axial compactness σ_e/λ_x. Only the radial compactness of the boundary pressure $k_{ac}r_j \ll 1$ has been assumed. For a comparison, the expression found by Crighton and Huerre [4] (Eq. (3.4)) for the acoustic field generated by a plane boundary pressure is recalled with our notations:

$$p(R, \theta) \sim \sqrt{2\pi} \sin\theta\, k_{ac} \hat{E}(k_{ac}\cos\theta - k_x) \frac{\exp(\mathrm{i}k_{ac}R - \mathrm{i}\frac{\pi}{4})}{\sqrt{k_{ac}R}}$$

The main differences with expression (7) are the $1/\sqrt{R}$ decay law and the $\sin\theta$ variation. Expression (8) of the near incompressible pressure field has been obtained for any boundary condition (1). Expression (9) is valid for a slowly modulated boundary pressure, i.e. $\sigma_e/\lambda_x \gg 1$.

In the next two sections, these results are used to discuss the experimental data [1].
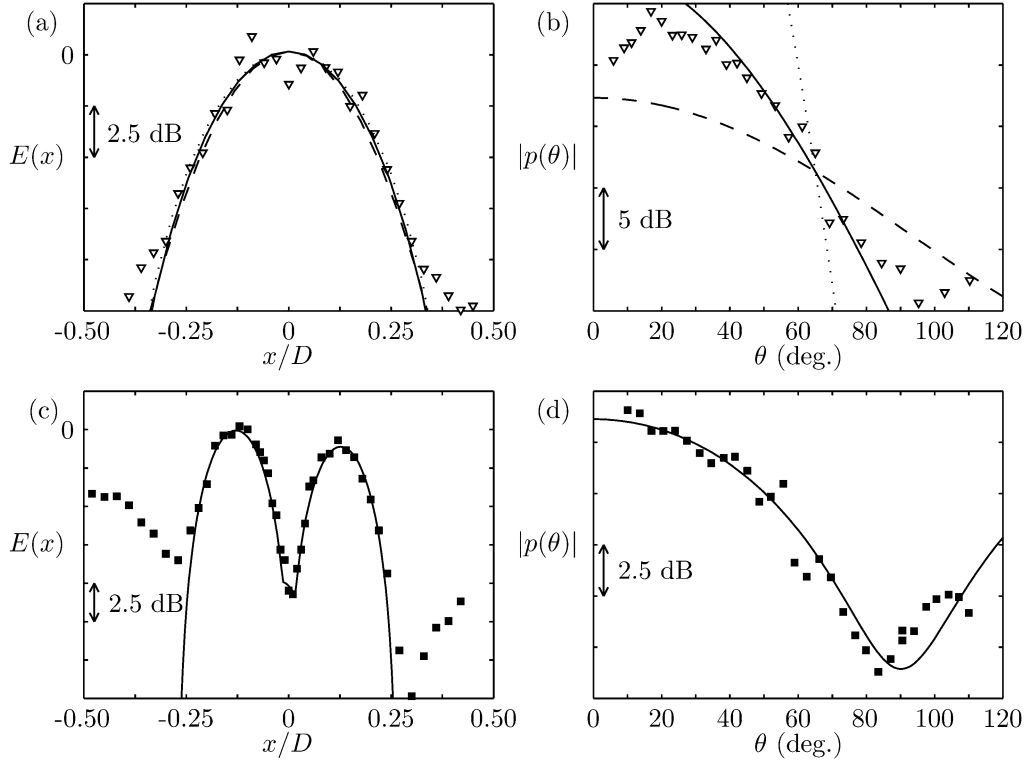
Fig. 1. Profiles of $E(x)$ at the boundary surface and corresponding directivity pattern $|p(\theta)|$. Top: $U_j = 40$ m·s^{-1}; $\triangledown$ experimental data; - - - Gaussian distribution p_2; — p_3; · · · p_4. Bottom: $U_j = 20$ m·s^{-1}; $\blacksquare$ experimental data; — sinusoidal distribution and model directivity (16).

Fig. 1. Profils de $E(x)$ sur la frontière et diagramme de directivité correspondant $|p(\theta)|$. En haut : $U_j = 40$ m·s^{-1} ; $\triangledown$ données expérimentales ; - - - distribution gaussienne p_2 ; — p_3 ; · · · p_4. En bas : $U_j = 20$ m·s^{-1} ; $\blacksquare$ données expérimentales ; — distribution sinusoïdale de pression proche et modèle (16).

3. Estimate of the far pressure field

The data given in [1] concerning the first subharmonic pressure field just outside the jet are recalled in Fig. 1(a) for the case $U_j = 40$ m·s^{-1}. A Gaussian distribution has been found to approximate this pressure field and the corresponding envelope $E(x)$ can be written:

$$E(x) = \exp\left(-\frac{x^2}{\sigma_e^2}\right) \tag{10}$$

where σ_e is the length-scale of the envelope function. The Fourier transform of $E(x)$ is given by:

$$\hat{E}(k) = \exp\left(-\frac{\sigma_e^2 k^2}{4}\right)$$

Expression (7) yields the acoustic directivity:

$$\left|p(R,\theta)\right| \propto \frac{1}{k_{ac}R}\exp\left(-\frac{\sigma_e^2 k_x^2}{4}D_\theta^2\right) \tag{11}$$

where $D_\theta = 1 - M_p \cos\theta$ is the Doppler factor and $M_p = k_{ac}/k_x$ is the phase Mach number. As found in [1], $M_p \ll 1$ and (11) can be expanded as follows:

$$\left|p(R,\theta)\right| \propto \frac{\exp(-\sigma_e^2 k_x^2/4)}{k_{ac}R}\exp\left(\frac{\sigma_e^2 k_x^2}{2}M_p \cos\theta\right) \tag{12}$$

This expression is similar to the expression found by Laufer and Yen [3]. However, with the measured values of the near pressure field given in Table 3 of [1], the experimental directivity pattern is badly recovered, as noticed in Fig. 1(b). The parameter $\sigma_e^2 k_x^2 / 2$ is indeed evaluated around 20, whereas a value of 45 is expected from the work of Laufer and Yen [3] and also by our measurements [1].

As proposed by Crighton and Huerre [4], other envelope functions can suitably approximate the near pressure field and in particular, $E_n(x)$ functions whose the Fourier transform is:

$$\hat{E}_n(k) = \exp\left(-\sigma_{en}^n |k|^n\right) \tag{13}$$

Their plot is represented in Fig. 1(a) for $n = 2$, 3 and 4. Note that $E_2(x)$ is the Gaussian distribution (10) with $\sigma_{e2} = \sigma_e / 2$. For $n \geqslant 3$, $E_n(x)$ has been computed numerically and σ_{e3} and σ_{e4} are found around $0.25 r_j$.

From expression (7), the resulting directivity is:

$$\left| p_n(R, \theta) \right| \propto \frac{1}{k_{ac} R} \exp\left(-\sigma_{en}^n k_x^n D_\theta^n\right)$$

and for $M_p \ll 1$:

$$\left| p_n(R, \theta) \right| \propto \frac{\exp(-\sigma_{en}^n k_x^n)}{k_{ac} R} \exp(n \sigma_{en}^n k_x^n M_p \cos\theta) \tag{14}$$

For $n = 3$, the attenuation coefficient $n \sigma_{en}^n k_x^n$ is found around the experimental value of 45 for the superdirective radiation and the directivity pattern plotted in Fig. 1(b) shows a good agreement with the data. The distribution $E_4(x)$ yields a sharper directivity with an attenuation coefficient of 150.

For $U_j = 20 \, \text{m·s}^{-1}$, the near pressure field of the first subharmonic is recalled in Fig. 1(c). The modulation function is constituted of two sinusoidal arches as in [1]:

$$E(x) = \cos\left(\pi \frac{x - x_{s1}}{\sigma_e}\right) B(x, x_{s1}, \sigma_e) + P_{21} \cos\left(\pi \frac{x - x_{s2}}{\sigma_e}\right) B(x, x_{s2}, \sigma_e) \tag{15}$$

where x_{s1} and x_{s2} are the axial locations of the arch maxima and P_{21} is the ratio of the amplitudes between the two pressure lobes. The boxcar function $B(x, x_{si}, \sigma_e)$ is equal to one for $|x - x_{si}| < \sigma_e / 2$ and zero otherwise. The envelope length-scale σ_e represents the size of one single arch. The Fourier transform of (15) is:

$$\hat{E}(k) = \left\{\exp(ikx_{s1}) + P_{21} \exp(ikx_{s2})\right\} \frac{\cos(k\sigma_e / 4)}{1 - (k\sigma_e / (2\pi))^2}$$

From expression (7), the acoustic directivity reads:

$$\left| p(R, \theta) \right| \propto \frac{1}{k_{ac} R} I(\theta) D_a(\theta) \tag{16}$$

where $D_a(\theta)$ is the radiation pattern for a single arch:

$$D_a(\theta) = \left| \frac{\cos(\frac{k_x \sigma_e}{2} D_\theta)}{1 - (\frac{k_x \sigma_e}{\pi})^2 D_\theta^2} \right|$$

and $I(\theta)$ takes into account the interference of the acoustic waves emitted from the two arches:

$$I(\theta) = \left| \exp(ik_x x_{s1} D_\theta) + P_{21} \exp(ik_x x_{s2} D_\theta) \right|$$

All the parameters involved in these expressions can be estimated with the data reported in [1] and the directivity (16) is plotted in Fig. 1(d). A good agreement with the measurements is noticed and in particular, the angle $\theta^\star$ of the minimum pressure is found around 90°. This extinction angle results of the destructive interference between the pressure waves emitted in phase opposition from the two arches. This is a straight consequence of the estimation made in [1] concerning the mean wave length $\lambda_x = 2\pi / k_x$ of the fluctuating pressure, whose half length $\lambda_x / 2$ has been identified to the distance between the top of the two arches $|x_{s2} - x_{s1}|$. A slight change in λ_x would indeed modify the location of $\theta^\star$. Furthermore, the shape of the directivity in the vicinity of $\theta^\star$ is sensitive to P_{21}. As the two pressure lobes have the same amplitude, i.e. $P_{21} = 1$, the pressure vanishes at $\theta^\star$.

4. Estimate of the near pressure field decay

Experimentally, the near subharmonic pressure field has been observed to decay exponentially from the center of the shear-layer, as recalled in Fig. 2(a) and (b). This result is compared to the pressure field predicted by the expression (8). The calculation has been performed numerically for the envelope functions $E_n(x)$, see the relation (13), and the modulation function (15).

For $U_j = 40$ m·s^{-1}, the near pressure field decay associated with $E_n(x)$ is displayed in Fig. 2(a). For $n = 2$, the agreement with the experimental data is not satisfactory. Indeed, it has been checked that the asymptotic expansion (9) is close in this case to the complete prediction of the pressure (8). Therefore, $|p(x,r)|$ varies as follows:

$$|p(x,r)| \propto \left(\frac{r_j}{r}\right)^{1/2} \exp\left(-k_x r - \frac{|x^2 - r^2|}{\sigma_e^2}\right) \tag{17}$$

This decay is mainly Gaussian and faster than the exponential evolution. As observed in Fig. 2(a), the decay of the near pressure field is nearly exponential for higher n values, $n = 3$ and $n = 4$, and is in a fair agreement with the data for large $|z|$ values. A contour plot of $|p(x,r)|$ is given in Fig. 2(b) for $n = 3$.

For $U_j = 20$ m·s^{-1}, the near pressure field associated to the sinusoidal envelope is plotted in Fig. 2(c). The agreement with the data is fairly good as $|z|$ is close to the boundary. The variation of this near pressure field is basically different from the previous superdirective case as shown by the contour plot of $|p(x,r)|$ in Fig. 2(d). The radiation by
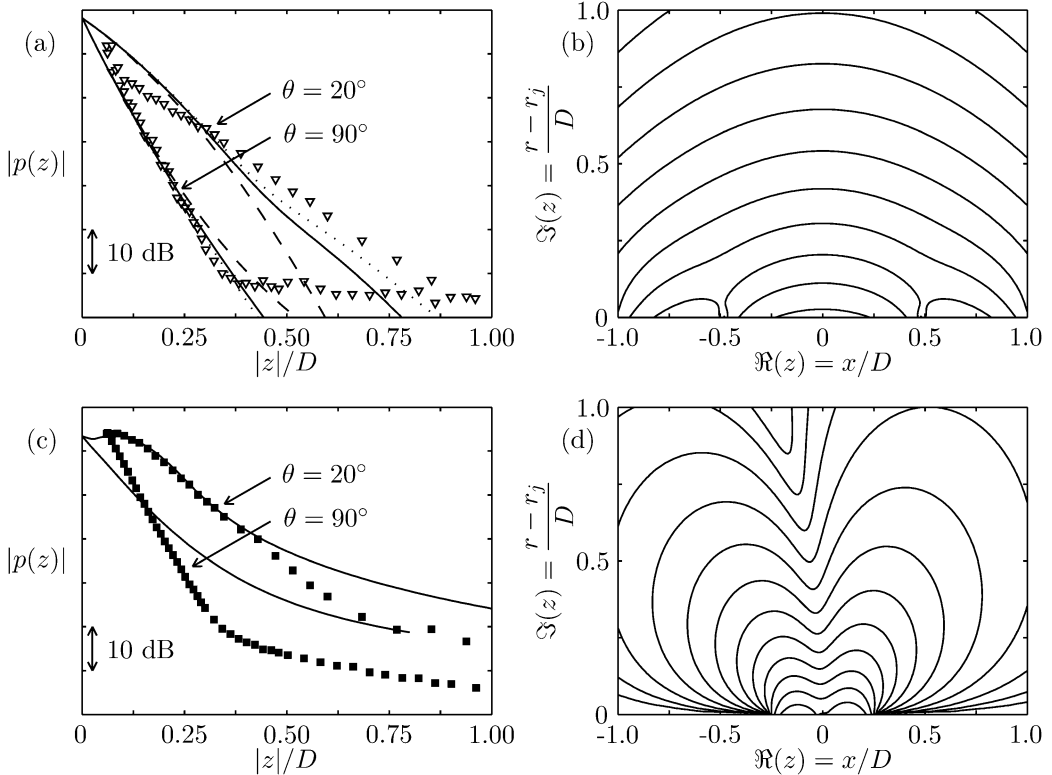
Fig. 2. Near pressure field decay. Top: $U_j = 40$ m.s^{-1}. (a): Comparison of the experimental data, symbols ∇, with various generalized Gaussian functions $E_n(x)$. - - - $p_2(z)$; — $p_3(z)$; $\cdots$ $p_4(z)$. (b): Contour plot of $p_3(x,r)$ with a step of 15 dB between iso-level lines. Bottom: $U_j = 20$ m.s^{-1}. (c): Comparison of the experimental data, symbols $\blacksquare$, with the two arches model (8), plotted in solid line —. (d): Contour plot of $p(x,r)$ with a step of 5 dB between iso-level lines.

Fig. 2. Décroissance de la pression en champ proche. En haut : $U_j = 40$ m·s^{-1}. (a) : Comparaison des mesures, symboles ∇, pour différentes fonctions gaussiennes généralisées $E_n(x)$. - - - $p_2(z)$; — $p_3(z)$; $\cdots$ $p_4(z)$. (b) : Lignes iso-niveau de $p_3(z)$ par pas de 15 dB. En-bas : $U_j = 20$ m·s^{-1}. (c) : Comparaison des mesures, symboles $\blacksquare$, avec le modèle constitué de deux arches (8), tracé en ligne solide —. (d) : Lignes iso-niveau de $p(x,r)$ par pas de 5 dB.

the two pressure lobes still prevails far from the boundary and seems to construct the far acoustic field stressed by the extinction angle $\theta^\star$.

5. Conclusion

The acoustic radiation from a cylindrical boundary pressure wave has been calculated. The far pressure field is given by the expression (7), obtained by using the assumption of compactness $k_{ac}r_j \ll 1$. The pressure field close to the boundary is provided by the expression (8) and for a slightly modulated source $\sigma_e k_x \ll 1$, by the asymptotic expression (9).

The superdirective far-field pattern has been recovered by using the envelope function $E_3(x)$, see expression (13), which is very close to the Gaussian shape found by Laufer and Yen [3]. The directivity of vortex pairing type has been retrieved with a near pressure field of sinusoidal form as proposed in [1]. In particular, an extinction angle has been predicted at $\theta^\star = 90°$, close to the experimental value of 85°. The experimental radial decay of the near pressure field has also been recovered.

Acknowledgements

References

[1] V. Fleury, C. Bailly, D. Juvé, Shear-layer acoustic radiation in an excited subsonic jet: Experimental study, C. R. Mecanique 333 (2005), in this issue.
[2] J.E. Bridges, Application of coherent structure and vortex sound theories to jet noise, Ph.D. Dissertation, University of Houston, 1990.
[3] J. Laufer, T.-C. Yen, Noise generation by a low-Mach-number jet, J. Fluid Mech. 134 (1983) 1–31.
[4] D.G. Crighton, P. Huerre, Shear-layer fluctuating pressure and superdirective acoustic sources, J. Fluid Mech. 220 (1990) 355–368.
[5] J.E. Bridges, F. Hussain, Direct evaluation of aeroacoustic theory in a jet, J. Fluid Mech. 240 (1992) 469–501.
[6] P.M. Morse, K.U. Ingard, Theoretical Acoustics, Princeton Univ. Press, Princeton, NJ, 1986, pp. 356–357.